Accelerated Cardiac MR Stress Perfusion with Radial Sampling After Physical Exercise with an MR-Compatible Supine Bicycle Ergometer

Silvio Pflugi,[1,2†] Sébastien Roujol,[1†] Mehmet Akçakaya,[1] Keigo Kawaji,[1] Murilo Foppa,[1] Bobby Heydari,[3] Beth Goddu,[1] Kraig Kissinger,[1] Sophie Berg,[1] Warren J. Manning,[1,4] Sebastian Kozerke,[2] and Reza Nezafat[1]*

Purpose: To evaluate the feasibility of accelerated cardiac MR (CMR) perfusion with radial sampling using nonlinear image reconstruction after exercise on an MR-compatible supine bike ergometer.

Methods: Eight healthy subjects were scanned on two separate days using radial and Cartesian CMR perfusion sequences in rest and exercise stress perfusion. Four different methods (standard gridding, conjugate gradient SENSE [CG-SENSE], nonlinear inversion with joint estimation of coil-sensitivity profiles [NLINV] and compressed sensing with a total variation constraint [TV]) were compared for the reconstruction of radial data. Cartesian data were reconstructed using SENSE. All images were assessed by two blinded readers in terms of image quality and diagnostic value.

Results: CG-SENSE and NLINV were scored more favorably than TV (in both rest and stress perfusion cases, $P < 0.05$) and gridding (for rest perfusion cases, $P < 0.05$). TV images showed patchy artifacts, which negatively influenced image quality especially in the stress perfusion images acquired with a low number of radial spokes. Although CG-SENSE and NLINV received better scores than Cartesian sampling in both rest and exercise stress perfusion cases, these differences were not statistically significant ($P > 0.05$).

Conclusion: We have demonstrated the feasibility of accelerated CMR perfusion using radial sampling after physical exercise using a supine bicycle ergometer in healthy subjects. For reconstruction of undersampled radial perfusion, CG-SENSE and NLINV resulted in better image quality than standard gridding or TV reconstruction. Further technical improvements and clinical assessment are needed before using this approach in patients with suspected coronary artery disease.
Magn Reson Med 74:384–395, 2015.

Key words: radial sampling; myocardial perfusion imaging; compressed sensing

INTRODUCTION

Coronary artery disease (CAD) remains the primary cause of death in the United States (1). Catheter-based diagnostic invasive X-ray coronary angiography remains the clinical gold standard for the diagnosis of significant CAD, with over 1 million catheter-based diagnostic X-ray coronary angiograms performed annually. However, only one third of patients undergoing elective cardiac catheterization without known diseases are diagnosed with significant CAD (2); therefore, better gatekeepers to invasive X-ray coronary angiography are still needed. Cardiac MR (CMR) perfusion at rest and stress is a noninvasive imaging approach, which allows assessment of functional significance of CAD (3–8). Both pharmacologic stress (vasodilators and beta agonists) and physiologic stress testing (treadmill and bicycle ergometer) have been used in CMR perfusion (9–14). Although pharmacologic stress has the advantage of providing uniformity in testing and a uniform vasodilator response, it cannot provide information regarding the patient's exercise capacity, hemodynamic response to exercise, and the extent of physical activity that can reproduce the patient's symptoms during imaging. To address these limitations, the feasibility of CMR imaging after physical exercise using a supine ergometer or treadmill has been demonstrated previously (12,13,15–20). However, exercise perfusion in CMR still has several notable challenges, which have limited its clinical use. Specifically, imaging after physical exercise must be performed as close as possible to the peak heart rate, which requires minimal transition time between the end of exercise and imaging. Furthermore, subjects are unable to hold their breath immediately after exercise, and imaging must be performed under free-breathing conditions. The acquisition of multiple slices using single-shot imaging with sufficient spatial and temporal resolution necessitates the use of accelerated imaging techniques, especially for stress CMR perfusion. Hence, CMR perfusion scans at rest and pharmacologic stress are commonly acquired with parallel imaging using either SENSE or GRAPPA with an acceleration factor of 2 (21–24). To further improve spatial or temporal

[1]Department of Medicine (Cardiovascular Division), Beth Israel Deaconess Medical Center and Harvard Medical School, Boston, Massachusetts, USA.
[2]Institute for Biomedical Engineering, University and ETH Zurich, Zurich, Switzerland.
[3]Department of Medicine, Brigham and Women Hospital and Harvard Medical School, Boston, Massachusetts, USA.
[4]Department of Radiology, Beth Israel Deaconess Medical Center and Harvard Medical School, Boston, Massachusetts, USA.
Grant sponsor: National Institutes of Health; Grant number: R01EB008743-01A2.
*Correspondence to: Reza Nezafat, Ph.D., Beth Israel Deaconess Medical Center, 330 Brookline Avenue, Boston, MA 02215. E-mail: rnezafat@bidmc.harvard.edu
Additional Supporting Information may be found in the online version of this article.
[†]Silvio Pflugi and Sébastien Roujol contributed equally to this study.
Received 11 October 2013; revised 30 June 2014; accepted 22 July 2014
DOI 10.1002/mrm.25405
Published online 8 August 2014 in Wiley Online Library (wileyonlinelibrary.com).

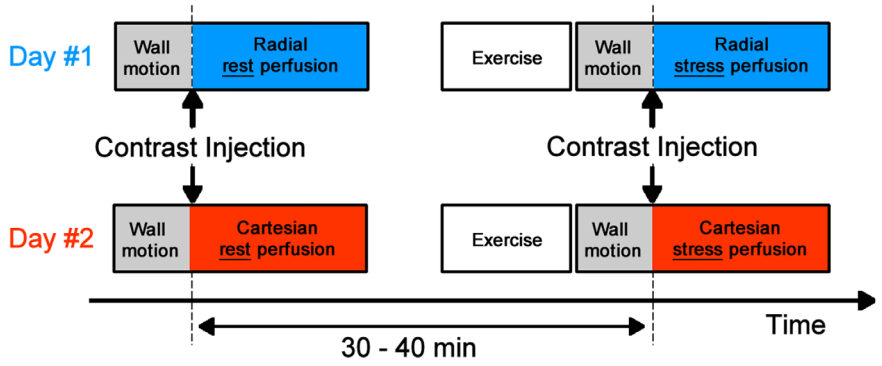

FIG. 1. Study protocol. Each subject was scanned twice on two separate days. Rest and exercise stress perfusion scans were performed using radial sampling (Day #1) and Cartesian sampling (Day #2). The order of rest and stress perfusion was randomized for Day #1 but kept for Day #2. A delay of 30–40 min was added between every injection to allow for contrast washout. A real-time cine scan (used for assessment of wall motion assessment) was acquired for 14 s before each perfusion scan.

resolution or coverage, spatiotemporal data correlations have also been exploited to accelerate data acquisition beyond parallel imaging (25–29). Compressed-sensing (CS) methods that exploit k-t sparsity of the data have also been recently used (30). However, the utilization of spatiotemporal correlations often requires breath-hold acquisitions to avoid respiratory-induced temporal blurring artifacts, and thus these methods cannot be used for free-breathing exercise stress perfusion. Furthermore, in parallel imaging, severe breathing motion results in misalignment between coil sensitivity map and imaging data and may also lead to reconstruction artifacts (31). Hence, in k-t–based reconstructions that acquire multiple coil elements, respiratory motion causes errors for both the coil sensitivity map generation and spatiotemporal correlation calculation.

Perfusion imaging is commonly performed using Cartesian sampling of k-space (32). Alternative sampling schemes (e.g., radial or spiral) have received attention recently for CMR perfusion due to their data acquisition efficiency and robustness with regard to motion (32–40). These sampling schemes have demonstrated the reduction of dark-rim artifacts in the myocardium, which are commonly observed in acquisitions with Cartesian sampling (41,42). The combination of radial sampling with improved reconstruction techniques such as HYPR (highly constrained back projection for time-resolved MRI) or model-based reconstructions enable higher acceleration, improved temporal resolution, and spatial coverage (35–37). Furthermore, the feasibility of three-dimensional perfusion was demonstrated recently using a radial stack-of-stars acquisition (34). Hence, accelerated non-Cartesian imaging has shown promise as an alternative to Cartesian sampling for CMR perfusion after physical exercise due to its 1) efficient k-space sampling, 2) better motion properties, and 3) lower dark-rim artifacts. However, the feasibility of using non-Cartesian CMR perfusion after physical exercise has yet to be demonstrated.

In this study, our first aim was to investigate the feasibility of an accelerated CMR perfusion using radial sampling after physical stress using a supine bicycle ergometer and to compare the image quality to images acquired using Cartesian sampling. Second, we evaluated the efficacy of nonlinear-based reconstruction techniques for undersampled radial perfusion acquired after physical exercise.

METHODS

All images were acquired on a 1.5T Philips Achieva scanner (Philips Healthcare, Best, The Netherlands) using a 32-channel cardiac phased array coil. The imaging protocol was approved by our institutional review board, and written informed consent was obtained from all participants. Eight healthy adult subjects (women, $n = 6$; men, $n = 2$; mean age, 25.7 ± 7.3 years) were recruited to undergo two CMR stress perfusion examinations with physical stress on two separate sessions that were at least 7 days apart. Figure 1 shows the protocol of the proposed study. In each session, subjects were scanned using the stress and rest protocols described below. All images were acquired using radial sampling (day 1) and Cartesian sampling (day 2). The order of rest and stress perfusion scans was randomized on day 1 for each subject. The selected order was kept constant for the day 2 session. A real-time radial steady-state free precession (SSFP) cine sequence was performed immediately following the bike exercise and prior to the perfusion scan for evaluation of wall motion abnormality, which was not investigated in this study.

Exercise Protocol

Exercise was performed using an MR compatible supine bike (Lode B.V, Groningen, The Netherlands) mounted on the MR table. After initial slice localization and coil sensitivity map calculation, the MR table was first moved out of the magnet bore while the subject remained in the supine position during bicycle exercise (Fig. 2). An exercise protocol was performed with initial ergometer resistance set to 25 W. The resistance was then increased every 2 min at 25-W increments to reach a target heart rate of ~140–150 bpm. Electrocardiographic rhythm and blood pressure were monitored throughout the exercise protocol. After completion of exercise, the MR table was immediately repositioned

FIG. 2. Supine ergometer setup. After an initial scout scan to localize the anatomy and prescribe the short axis slices, each subject was slid out of the scanner while still lying on the scanner bed. This was followed by the exercise protocol before sliding the subject back into the magnet bore to start the scanning sequence. A CMR nurse controlled the level of exercise and continuously monitored each patient's heart rate and blood pressure, while two MR technologists communicated with the subject, initiated the scanning, and injected the contrast agent using a MEDRAD Spectris Solaris EP MR injection system (MEDRAD, Inc., Warrendale, Pennsylvania, USA).

into the magnet bore for imaging. To enable rapid scanning, two experienced technologists initiated a 14-s real-time cine scan followed by a stress perfusion scan from inside the MR scanner room.

Imaging Protocol

A real-time linear radial SSFP cine sequence was acquired for assessment of wall motion over 14 s. This was immediately followed by an injection of 0.05 mmol/kg of gadopentetate dimeglumine (Magnevist; Bayer Schering Pharma AG, Berlin, Germany) and the CMR perfusion sequence was initiated ~20 s after peak exercise.

Radial perfusion imaging was performed using a radial SSFP sequence with a 90° saturation preparation pulse. Three slices were acquired per heartbeat in the short axis orientation. The imaging parameters were as follows: pulse repetition time/echo time/$\alpha = 2.78$ ms/1.39 ms/50°; field of view = 300 × 300 mm^2; resolution = 2.2 × 2.2 × 10 mm^3; half alpha; fixed angle between each consecutive spoke = 180°/spoke number; and 88 dynamics per slice. The saturation recovery time (from the saturation pulse to the middle of the readout) was 100 ms. The temporal resolution was ~120 ms for rest perfusion and ~62 ms for stress perfusion. This corresponded to the acquisition of 43 radial spokes (net acceleration factor = 5) and 22 radial spokes (net acceleration factor = 9.7) for rest and stress perfusion, respectively. The overall acquisition time was ~185 ms for rest perfusion and ~155 ms for stress perfusion.

For Cartesian perfusion imaging, an SSFP sequence with a 90° saturation preparation pulse was used to acquire three slices in the short axis orientation using the following parameters: pulse repetition time/echo time/$\alpha = 2.91$ ms/1.45 ms/50°; field of view = 320 × 320 mm^2; resolution = 2.2 × 2.2 × 8 mm^3; half alpha; half Fourier (factor = 0.75); number of phase encoding lines = 41 for rest and 32 for stress; and 65 dynamics per slice. The saturation recovery time (from the saturation pulse to the acquisition of the k-space center line) was 100 ms for rest perfusion and 72 ms for stress perfusion. The temporal resolution was ~120 ms for rest perfusion and ~93 ms for stress perfusion. It should be noted that we reduced the saturation recovery delay and increased the acquisition window of the Cartesian stress acquisition to enable the use of reasonable SENSE factor because we found in preliminary results that a SENSE acceleration rate ≥4 led to severe reduction of image quality (43). The resulting SENSE rate (R) for the Cartesian scans was R = 2.75 acceleration for rest perfusion and R = 3.5 acceleration for stress perfusion. Similar to radial scans, the overall acquisition time was ~185 ms for rest perfusion and ~155 ms for stress perfusion.

An improved slice tracking technique (44) was used for both rest and exercise stress perfusion protocols. In this approach, the location of each slice is adjusted independently based on a two-dimensional pencil beam navigator acquired before the imaging pulses of each slice and a tracking factor of 0.6. A navigator restore pulse is also applied after each saturation pulse to prepare the navigator signal (44). The duration of the NAV restore pulse, the NAV pulse, and the NAV computation was ~30 ms. All scans used the longest possible trigger delay to enable the acquisition of the three slices at the end of the RR interval.

Image Reconstruction

The Cartesian reconstructions were performed on the scanner using commercially available reconstruction software which uses coil sensitivity maps generated from a pre-scan acquired before each CMR perfusion protocol.

All raw k-space data for radial perfusion were extracted for off-line reconstruction and analysis. All radial reconstructions were performed without any sharing of radial spokes across cardiac cycles. All radial reconstructions were performed off-line using MATLAB (MathWorks, Natick, Massachusetts, USA). Undersampled radial data were reconstructed using the four reconstruction methods described below: 1) gridding, 2) conjugate gradient SENSE (CG-SENSE), 3) CS with first-order total variation constraint (TV), and 4) regularized nonlinear inversion with joint estimation of coil-sensitivity maps (NLINV).

Gridding

Standard gridding was performed using Fessler and Sutton's NUFFT (nonuniform fast-Fourier transform) package (45). The default minimum-maximum interpolator with Kaiser-Bessel scaling factors was used with a 6×6 neighborhood. To combine information from all coil elements, the k-space data of each coil was gridded separately and the final reconstruction was obtained by taking the root-sum-squares of all gridded coil images.

CG-SENSE

A linear parallel imaging reconstruction was performed using CG-SENSE (46) for a fixed number of iterations ($n = 3$). Coil sensitivity maps were estimated separately for each heartbeat using Hanning filtering on central k-space (47), where the number of center points was chosen to fulfill the Nyquist criterion. In each conjugate gradient iteration, both the system matrix (i.e., multiplication of the combined image with the coil sensitivity maps followed by inverse gridding in each coil) and the adjoint system matrix (i.e., gridding in each coil followed by multiplication of the complex conjugate of the coil sensitivities and subsequent summation in the coil dimension) were applied during the calculation of the residual and the conjugate gradient step as described by Block et al. (46). A preconditioner based on the Jacobi preconditioner (48) was calculated by the gridding and inverse gridding of a matrix containing all ones and was utilized for faster convergence of the CG algorithm (48). The number of iterations was determined by visual assessment of image quality to achieve a good trade-off between aliasing artifacts and enhanced noise in the image as demonstrated by Qu et al. (49). Visual assessment of intermediate images after 3–7 iterations was performed in one subject for both rest and stress perfusion images. There was visually almost no difference between three, four, or five iterations in both rest and stress perfusion. However, each iteration tends to increase the noise level. Three iterations were visually assessed as optimal for rest and stress perfusion images and were used for the CG-SENSE reconstruction of all scans. Intensity correction was performed at the end by multiplying the resulting image by the root-sum-squares of all coil sensitivity maps.

CS with First-Order TV

The iterative compressed sensing implementation used a first-order total variation regularization term as follows (47):

$$\vec{x} = \arg\min_{\vec{x}} \frac{1}{2}||A\vec{x} - \vec{y}||_2^2 + \lambda \cdot \sum\nolimits_i R_i(\vec{x}) \qquad [1]$$

where $\vec{x}$ is the final image, $\vec{y}$ is the acquired k-space data, and **A** is the system matrix, which involves multiplication of the image with the coil sensitivity maps, followed by a Fourier transform and inverse gridding onto the radial spokes, as described by Block et al. (47). An additional constraint on image data positiveness was utilized by Block et al. to flatten phase variations of spin echo data across the field of view. Because the issue of phase variations was not applicable in our study, this term was not used in the employed TV reconstruction. A total variation approach was taken for the regularizer $R_i(\vec{x})$ used to reconstruct the final image in this study as

$$R_i(\vec{x}) = \sqrt{D_x(x_i)^2 + D_y(x_i)^2 + eps} \qquad [2]$$

in which D_x and D_y represent the first-order spatial finite differences in the first and second dimensions of the image, respectively, and *eps* is a smoothing parameter set to 10^{-15}, which is less than 10^{-18} times the maximum absolute value of the image (50). The employed TV reconstruction did not integrate a second-order term (47).

Coil sensitivity maps used in the system matrix A were obtained via the iterative nonlinear conjugate gradient method applied to each coil image separately, with a smoothing regularizer given by $R_{coil}(\vec{x}) = D_x(x_i)^2 + D_y(x_i)^2$ (47). The weighting factor for the square penalty on the image derivatives was set to 10 times the maximum intensity value of the image. Twenty iterations were used to obtain smooth coil sensitivity maps. Subsequently, the total variation regularized least squares problem in Equation [1] was solved using these coil sensitivities. The weighting factor λ for the total variation penalty was fixed to be 0.0005 times the maximum intensity value of the image, and the number of iterations was set to 60. As an additional regularizer, the field of view was restricted using a binary circular mask. The NUFFT gridding package was used for gridding and inverse gridding.

Regularized NLINV

In this technique, the coil-sensitivity maps c_i are treated as unknowns and are jointly estimated with the image ρ (51). The operator G outputs the measurements in all the coils as

$$\vec{y} = G\begin{pmatrix} \rho \\ c_1 \\ \vdots \\ c_N \end{pmatrix} = G(\vec{x}). \qquad [3]$$

A nonlinear least squares problem is solved using a weighted Tikhonov regularization,

$$||\vec{y} - G(\vec{x})||_2^2 + ||W\vec{x}||_2^2, \qquad [4]$$

where the weights matrix W penalizes high frequencies with a polynomial of degree l in the distance to the k-space center to enforce smooth coil maps (51):

$$\hat{x} = \begin{pmatrix} \rho \\ \hat{c}_1 \\ \vdots \\ \hat{c}_N \end{pmatrix} = \begin{pmatrix} I & & & \\ & (1+||\vec{k}||^2)^{l/2}F & & \\ & & \ddots & \\ & & & (1+||\vec{k}||^2)^{l/2}F \end{pmatrix} \begin{pmatrix} \rho \\ c_1 \\ \vdots \\ c_N \end{pmatrix} = W\vec{x} \quad [5]$$

Here, F represents the Fourier transform and $\vec{k}$ represents the k-space coordinates. These sets of equations are solved using the iterative regularized Gauss–Newton method, wherein the following minimization is performed at each Newton step:

$$||DG(\hat{x}_n)d\hat{x} - (\vec{y} - G(\hat{x}_n))||^2 + \alpha_n||\hat{x}_n + d\hat{x} - \hat{x}_0||^2 \quad [6]$$

Here, DG is the derivative of the operator G and $d\hat{x}$ is the update that requires solving. The regularization parameter α_0 was initialized to 1 and is reduced in every iteration as

$$\alpha_n = \alpha_0\left(\frac{2}{3}\right)^n.$$

A fixed number of iterations was used for the NLINV reconstruction of all scans. The number of iterations was selected by visual assessment of intermediate images after 3–7 iterations. The optimal image quality was obtained between 4 and 5 iterations, whereas a severe reduction of image quality was observed with more than 5 iterations. Therefore, the number of iterations for NLINV was fixed to 4 for both rest and stress perfusion images.

Parameter calibration in CG-SENSE and NLINV based on visual assessment was performed independently by a third reader, which may mitigate this effect. The optimized parameters were then kept constant for all subjects and scans.

Data Analysis and Statistics

The contrast enhancement ratio (CER) was measured for the four radial reconstruction methods for both rest and stress perfusion datasets. CER was defined as:

$$CER = \frac{S_{mpi} - S_{baseline}}{S_{baseline}} \quad [7]$$

where S_{mpi} is the average myocardial signal measured in the frame with maximal myocardial intensity and $S_{baseline}$ is the average myocardial signal measured in a frame acquired before contrast arrival. S_{mpi} and $S_{baseline}$ were measured using two separate regions of interest encompassing most of the left ventricular myocardium. Because CER data are continuous variables and assumed to follow a Gaussian distribution, parametric tests were used for statistical analysis. The statistical significance in CER between the four radial reconstruction methods was evaluated using one-way analysis of variance with a significance threshold of $P < 0.05$. Additional paired t tests with Bonferroni correction were performed for all pairs of reconstruction methods when the analysis of variance test was found to be significant. Statistical significance was considered at $P < 0.05/6 = 0.008$.

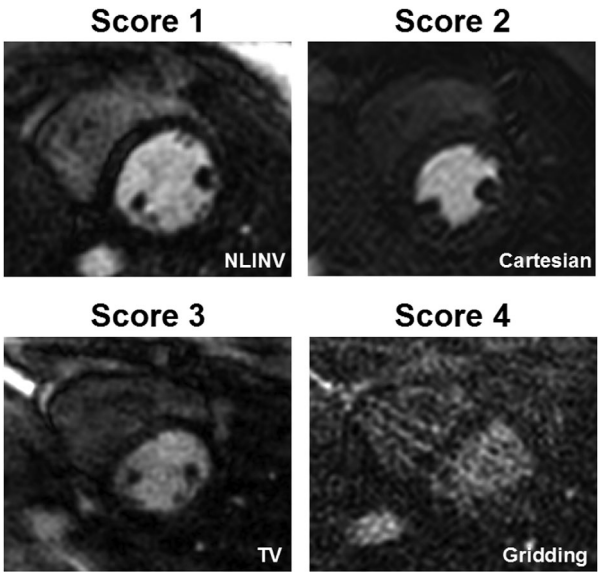

FIG. 3. Example of subjective image quality scores for NLINV, Cartesian imaging, TV, and gridding.

Two experienced cardiologists who were blinded to subject information and acquisition scheme independently performed a subjective qualitative assessment of image quality. The subjective image score was performed using only the most basal slice in order to keep the data analysis feasible in a reasonable amount of time. All four radial reconstructions were displayed simultaneously on the screen, where the operator was able to scroll through the temporal dynamics, zoom, and adjust the window level. The Cartesian images were shown separately. For each data set, diagnostic image quality was assessed using a dichotomous "yes" or "no" question. The diagnostic image quality was defined as the confidence of visualization of enhancement in the sub-endocardial territory of the left ventricular myocardium, and therefore the confidence one would have had if a defect had been present. Overall image quality of perfusion was also evaluated by using a single score for the entire dynamic sequence on a four-point scale: 1 = excellent, 2 = good, 3 = fair, and 4 = poor. The readers were instructed to include signal-to-noise ratio (SNR), contrast-to-noise ratio (CNR), clarity of myocardial border, and motion artifacts for scoring the overall image quality. Examples of image quality score are shown in Figure 3. The subjective scores were averaged from the two readers and are presented as the mean ± standard deviation. The median of the two scores was also reported. Subjective scores, which are discrete variables, were compared using nonparametric Wilcoxon signed rank tests. We note that due to our small sample size (n = 8 for rest and n = 6 for

Table 1
CER Obtained for Rest and Stress Perfusion

	Gridding	CG-SENSE	NLINV	TV
Rest perfusion	0.17 ± 0.08	1.94 ± 1.31	1.91 ± 1.00	1.04 ± 0.43
Stress perfusion	0.17 ± 0.1	3.84 ± 3.30	3.5 ± 2.1	0.97 ± 0.61

Higher CER values were obtained with CG-SENSE and NLINV when compared with gridding and TV for rest and stress perfusion.

stress), we did not perform the Bonferroni correction for evaluation of statistical significance. $P < 0.05$ was considered statistically significant. The diagnostic value was reported for each individual reader.

RESULTS

All eight subjects were able to tolerate the level of exercise and reach the target heart rate of 140 bpm. Rest perfusion imaging was performed successfully in all subjects; however, stress perfusion data were collected successfully in six out of eight subjects across the two sessions, where two scans failed due to technical problems and scan time constraints. In the first unsuccessful subject, the exercise bike perfusion protocol was terminated immediately after contrast injection due to an inaccurate navigator signal coming from misalignment in patient position from the prescribed anatomical position after exercise. Time limitations prohibited the repetition of this scan. In the second subject, our scanner hardware encountered a system error prior to stress perfusion imaging, resulting in an early termination of the examination protocol, and further rescheduling of the subject to repeat this scan was not feasible. The failed stress cases were not included in the final comparison study.

Table 1 shows the CER measurements obtained in rest and stress perfusion cases. There was a statistical difference in CER between all radial reconstruction methods for both rest perfusion ($P < 0.001$) and stress perfusion cases ($P = 0.003$). P values obtained for each subsequent paired-wise t test are shown in Supporting Table 1. CG-SENSE and NLINV provided higher CER measurements

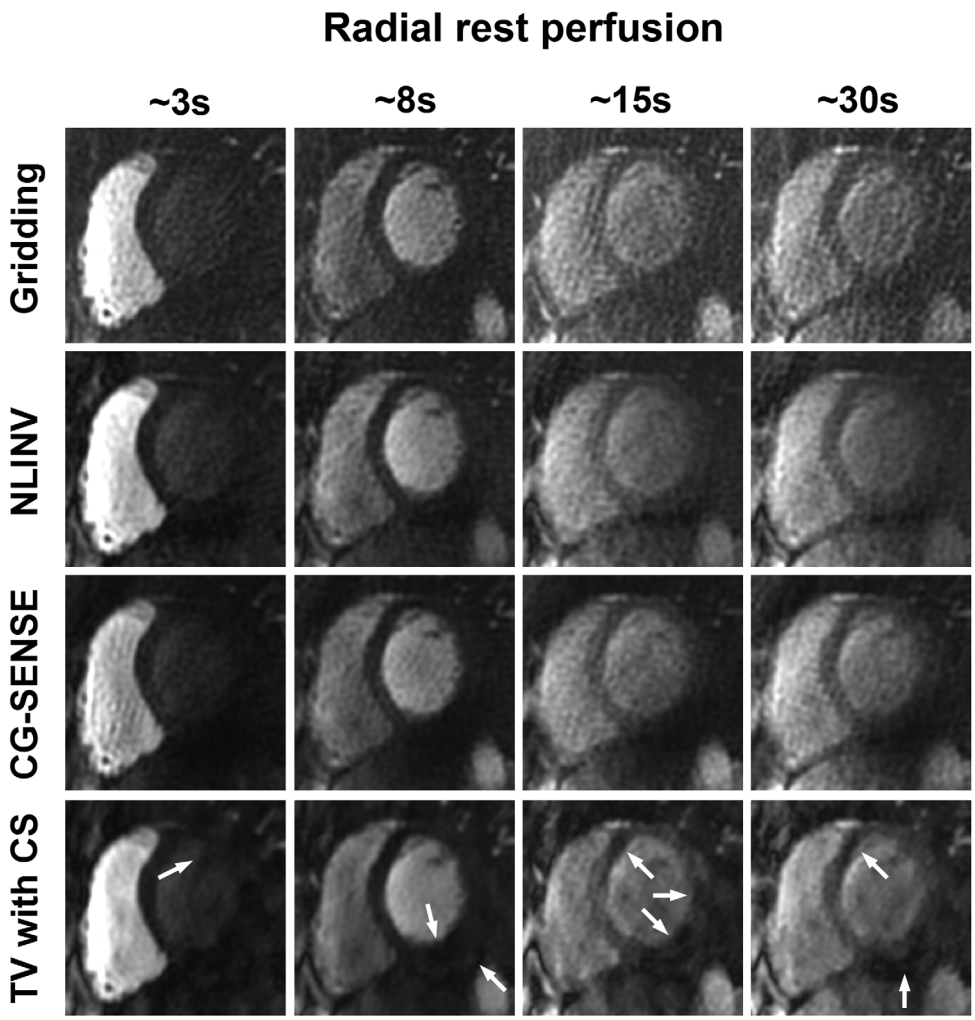

FIG. 4. Comparison of the four reconstruction methods for a dataset acquired using the undersampled radial rest perfusion sequence. Four different temporal frames acquired at 3, 8, 15, and 30 s after contrast arrival in the right ventricle are shown. Examples of patchy artifacts are shown for the TV reconstruction (arrows).

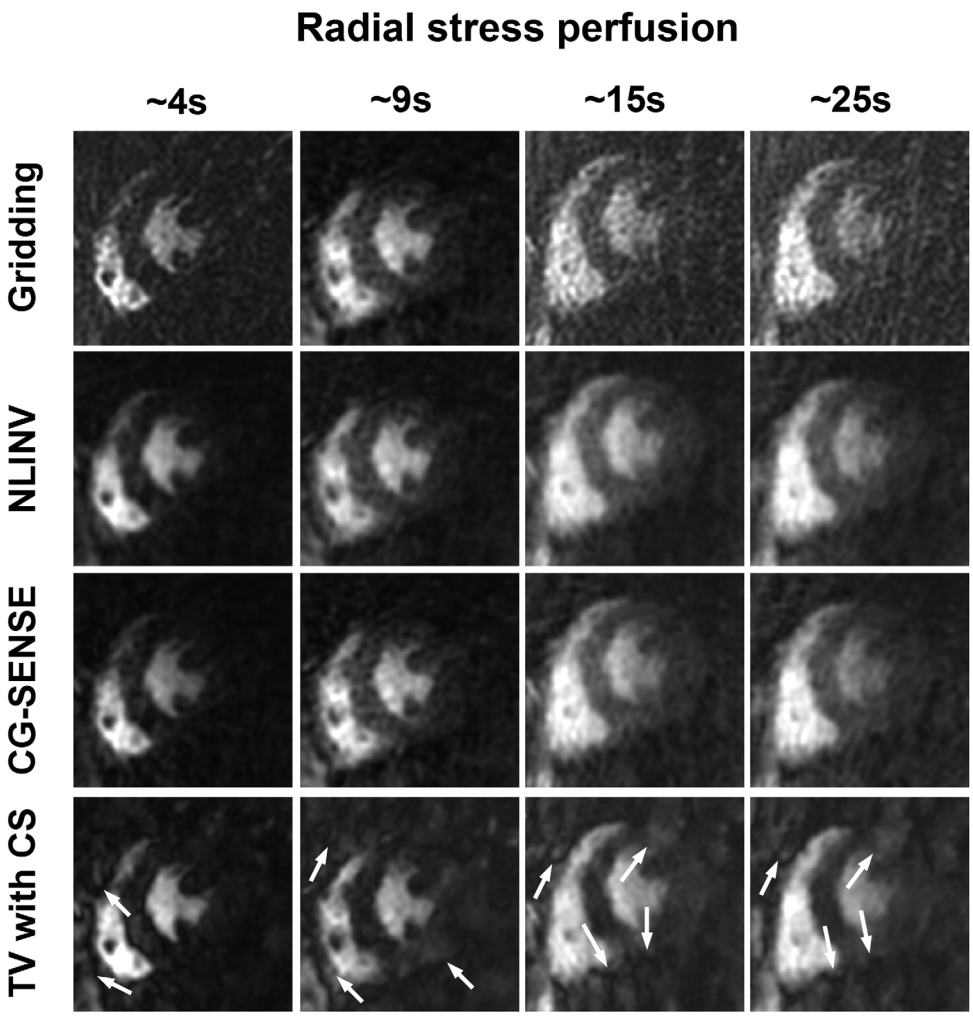

FIG. 5. Comparison of the four reconstruction methods using the radial stress perfusion sequence. Four different temporal frames acquired at 4, 9, 15, and 25 s after arrival of contrast bolus in the right ventricle are shown. Examples of patchy artifacts are shown for the TV reconstruction (arrows).

than gridding and TV for both rest ad stress perfusion (all corresponding $P < 0.05$). There were no statistical differences in CER between CG-SENSE and NLINV for rest perfusion ($P = 0.9$) or stress perfusion ($P = 0.53$).

Figures 4 and 5 show four reconstructions of radial perfusion data acquired at four different dynamics (at 3, 8, 12, and 16 s after contrast arrival in the right ventricle) during rest and stress perfusion, respectively. Supporting Information movies 1 to 4 show each reconstruction method corresponding to the stress perfusion case in Figure 5. Images acquired during stress perfusion have inferior image quality than images acquired during rest perfusion. Gridding images show streaking artifacts and higher noise level, especially for stress perfusion, whereas the TV reconstruction yields patchy images. For both rest and stress perfusion, CG-SENSE and NLINV reconstruction methods show superior results compared with gridding and TV.

Figures 6 and 7 show head-to-head comparisons between the radial and Cartesian sequence at rest and after exercise stress, respectively. Cartesian and radial NLINV reconstruction yielded comparable image quality for rest perfusion. However, Cartesian sampling led to fold-over artifacts and higher noise compared with radial sampling for stress perfusion imaging.

Table 2 and Supporting Table 2 show the subjective image scores assessed by the two readers and the associated P values, respectively. For rest perfusion, NLINV was scored significantly higher than gridding ($P = 0.021$) and TV ($P = 0.011$), and CG-SENSE was scored significantly higher than TV ($P = 0.039$). There was also a trend for CG-SENSE to receive better score than gridding ($P = 0.07$). There were no statistical differences between Cartesian sampling and any of the radial reconstruction methods ($P > 0.1$ for all comparisons). All images with NLINV and CG-SENSE reconstruction (8/8) were assessed as diagnostic by both readers; however, gridding, CS-TV, and Cartesian images were determined to be diagnostic in 6 out of 8 cases.

For stress perfusion, NLINV and CG-SENSE were scored higher than TV ($P = 0.009$ and $P = 0.004$, respectively). There was a trend for gridding to receive higher score than TV ($P = 0.06$). Cartesian sampling was scored higher than TV ($P = 0.043$). There were no other statistically significant differences among the remaining pairedwise comparisons ($P > 0.05$).

Table 3 shows the diagnostic image quality obtained with all reconstruction methods. CG-SENSE images were diagnostic in 5 out of 6 cases by both readers. NLINV was judged to be diagnostic in 5 cases by the first reader

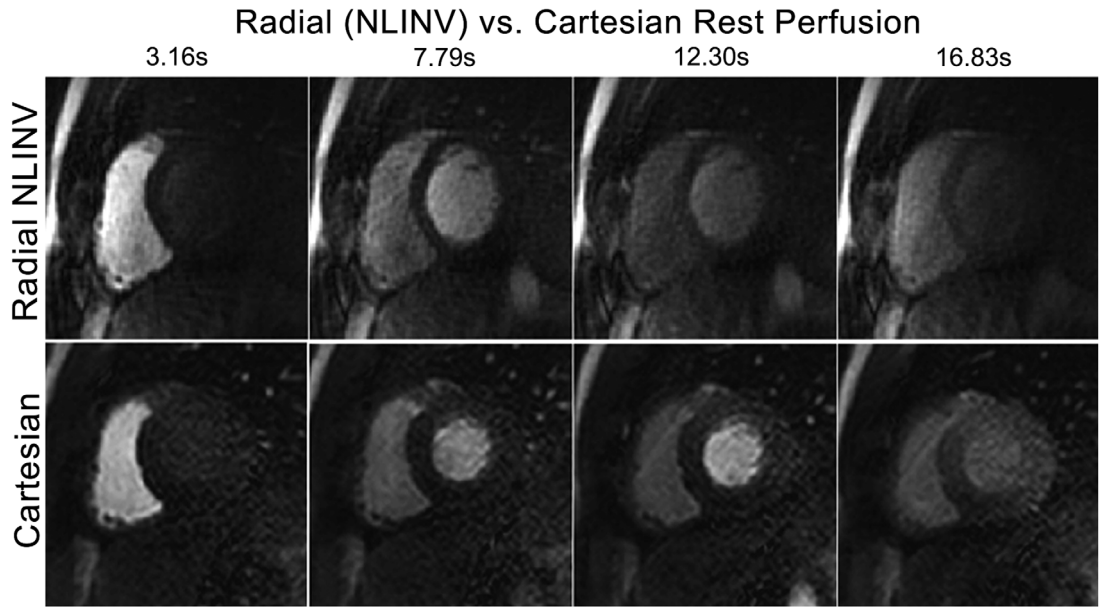

FIG. 6. Comparison between radial and Cartesian rest perfusion at four different temporal dynamics during the first pass of the contrast bolus. The radial images were reconstructed using NLINV; Cartesian images were reconstructed online on the scanner.

and in all 6 cases by the second reader. TV images received the worst scores in terms of overall image quality from both readers and were only diagnostic in 1 case by reader 1. Reader 2 determined that all cases were nondiagnostic = 0. For gridding, 4 cases (reader 1) and 2 cases (reader 2) were diagnostic. Finally, 4 cases (reader 1) and 5 cases (reader 2) were assessed as diagnostic for the Cartesian reconstruction.

DISCUSSION

In this study, we demonstrated the feasibility of CMR perfusion after physical exercise using a supine bicycle ergometer with accelerated radial image acquisition, which were compared with Cartesian sampling using the same protocol on a separate day. We also investigated the utility of four different reconstruction strategies to reduce the streaking artifacts resulting from undersampled radial sampling. However, none of the techniques provided a 100% diagnostic value for both rest and stress perfusion imaging, which is a concern for the direct applicability of these methods in patients. Further developments are warranted to improve image quality and the diagnostic value of the images.

The majority of rest and pharmacological CMR perfusion examinations are performed during a breath-hold. However, breath holding is not feasible after physical stress, even in healthy subjects. In our experience, this is

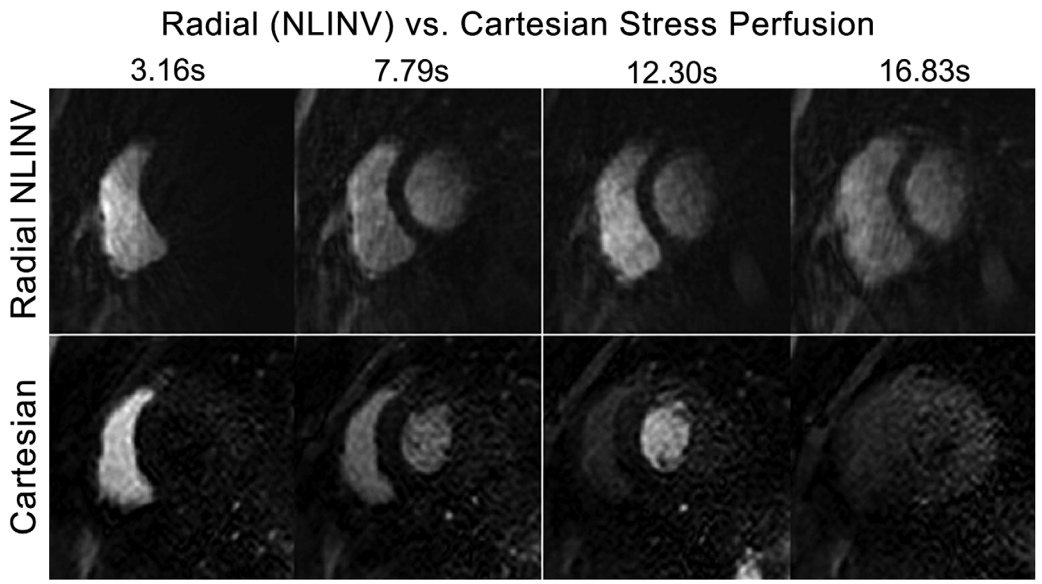

FIG. 7. Comparison between radial and Cartesian stress perfusion at four different temporal dynamics during the first pass of the contrast bolus. The radial images were reconstructed using NLINV; Cartesian images were reconstructed online on the scanner.

Table 2
Overall Image Quality Obtained for Rest and Stress Perfusion

	Gridding	CG-SENSE	NLINV	TV	Cartesian
Rest perfusion	1.88 ± 0.72 (2)	1.50 ± 0.63 (1)	1.38 ± 0.62 (1)	2.00 ± 0.73 (2)	1.81 ± 0.75 (2)
Stress perfusion	2.83 ± 0.83 (3)	2.25 ± 0.62 (2)	2.25 ± 0.87 (2)	3.42 ± 0.51 (3)	2.50 ± 1.16 (2.5)

Data are presented as the mean ± standard deviation (median). For rest perfusion, there were statistically significant differences between gridding and NLINV ($P = 0.021$), CG-SENSE and TV ($P = 0.039$), and NLINV and TV ($P = 0.011$). For stress perfusion, there were statistically significant differences between CG-SENSE and TV ($P = 0.004$), NLINV and TV ($P = 0.009$), and TV and Cartesian sampling ($P = 0.043$).

one of the major technical limitations of CMR perfusion after physical stress. In order to address postexercise respiratory motion during perfusion imaging, our method incorporated a diaphragmatic respiratory navigator tracking in combination with slice following to reduce the respiratory-induced motion (44). A fixed tracking factor of 0.6 was used for all subjects and may have limited the performance of the slice tracking technique (52,53). In addition, the slice tracking technique might have performed differently for Cartesian acquisition and radial acquisitions due to their different temporal sampling strategies and timing of the k-space center lines. For Cartesian sampled images, a spatial resolution that necessitates a SENSE acceleration rate of <4 was selected. In our preliminary stress perfusion study (43), Cartesian perfusion imaging using a SENSE acceleration rate of 4 yielded poor image quality. Therefore, an acceleration rate of 3.5 for stress perfusion to allow the coverage of 3 slices with reasonable spatial resolution was selected. However, even with a 32-channel cardiac phased-array coil, the g-factor penalty of using such acceleration with two-dimensional imaging is very high and would result in imaging artifacts and noise amplification.

The same set of reconstruction parameters was used for each method in both rest and stress perfusion imaging despite different number of spokes and acceleration factor. However, tailored optimizations for either rest-only or stress-only perfusion cases may lead to improved reconstruction. However, since the calibration of NLINV and CG-SENSE was performed by visual assessment, this could have led to a potential bias toward these methods.

In this study, the gridding reconstruction suffered from streaking artifacts in both rest and exercise stress perfusion scans. The conventional gridding reconstruction does not utilize additional information beyond sampled points for recovering the missing undersampled k-space data. Therefore, the inferior performance compared with NLINV and CG-SENSE and Cartesian was expected. The CS-based reconstructed images were not scored favorably by either of the blinded readers. TV regularization resulted in patch-like artifacts in the images with reduced streaking artifacts. However, both readers preferred streaking artifacts compared with patchy CS-reconstructed images. This is consistent with a recent study, which also showed inferior image quality of CS reconstructed images for images acquired with lower spatial resolution and high acceleration (54). The performance of the TV-based reconstruction is best when resulting artifacts are thin structures. However, the highly undersampled radial data in this study result in relatively wide streaks and the TV reconstruction penalizes oscillations while preserving sharp edges (47). Because prior CS-based reconstruction for perfusion imaging (30,33,34) exploited the temporal correlation of perfusion data, we cannot directly compare our results with those of prior studies. Further studies to investigate other CS-based reconstruction are needed.

Table 3
Rate of Diagnostic Dataset as Assessed by Each Reader for Rest and Stress Perfusion

	Gridding	CG-SENSE	NLINV	TV	Cartesian
Rest perfusion					
Reader #1	8/8	8/8	8/8	8/8	8/8
Reader #2	6/8	8/8	8/8	6/8	6/8
Stress perfusion					
Reader #1	4/6	5/6	4/6	1/6	4/6
Reader #2	2/6	5/6	6/6	0/6	5/6

CG-SENSE and NLINV reconstruction methods provided the best diagnostic rate for both rest and stress perfusion.

The range of CER measurements was found much lower for gridding and TV than CG-SENSE and NLINV. The gridding reconstruction led to the lowest CER among the four methods and could be explained by two factors. First, this reconstruction method does not have any mechanism to estimate the missing k-space information, and second, the images are associated with a high level of streaking artifacts. The TV reconstruction also led to substantially lower CER than NLINV and CG-SENSE, which could potentially be explained by its inherent spatial smoothness constraint, which penalizes high spatial signal variations in the reconstructed images.

Because it is a complicated task to measure the true spatial resolution of the employed radially reconstructed images, the reported spatial resolution corresponded to the field of view divided by the acquisition matrix size. Due to the high employed acceleration factor, it is difficult to guarantee that the true spatial resolution will be equal to the reported one. Indeed, the true spatial resolution of radially reconstructed images may likely be inferior to the reported spatial resolution.

All Cartesian images were reconstructed with the vendor-provided SENSE reconstruction and processing, which typically may apply more sophisticated image filtering and denoising, resulting in superior image quality when compared with our in-house reconstructed images, creating a bias toward image quality of these scans. A high acceleration factor for SENSE had to be selected for Cartesian imaging to enable the acquisition of three slices per heartbeat at high heart rates. However, these acceleration factors were higher than the one commonly

used in CMR perfusion and may have contributed to the reduced image quality of Cartesian data. The pulse repetition time and the spatial resolution of the Cartesian scans were different which may adversely affect image quality compared to radially acquired images. In addition, the temporal resolution and the saturation recovery delay for stress scans were different between radial and Cartesian acquisitions. The former leads to a favorable condition for Cartesian imaging due to the longer acquisition window, whereas the latter affects the radial acquisition more favorably, since the SNR is higher due to the longer saturation recovery delay. Therefore, it is difficult to characterize which of these effects is more important in the final reconstruction.

To allow free movement, the subject has to be pulled out of the scanner bore for exercising. During exercise, the coil and subject's location may change relative to the starting position, resulting in changed slice localizations and possible artifacts. In those cases, the accuracy of the preacquired coil sensitivity maps will be degraded (55) and may result in artifacts in the reconstructed Cartesian data.

Unlike other accelerated perfusion methods, this study did not examine reconstruction methods that incorporated temporal correlation of the perfusion data in the reconstruction step. This is to account for increased respiratory motion after physical exercise, which induce additional temporal blurring and reconstruction-based artifacts caused by imperfect coil sensitivities during significant breathing motion. This limits the acceleration rate that can be achieved when compared with k-t–based approaches. Several recent studies have proposed to simultaneously combine the motion correction problem with the reconstruction of undersampled data (25,35,56,57). After exercise, the amount and changes in breathing pattern is quite substantial; therefore, these techniques may not be robust enough for perfusion imaging after exercise. Further studies are warranted to determine whether such combined approaches can be used to improve image quality.

In this study, quantitative CMR perfusion measurements were not performed. SNR and CNR were not evaluated, because the compressed sensing reconstruction thresholds and shrinks the noise and would bias the SNR and CNR analysis. Similarly, NLINV is a nonlinear reconstruction method, and it is not clear how the SNR/CNR measurements can be performed for this approach. The study protocol, which used a single-injection first-pass perfusion, did not allow us to calculate myocardial perfusion reserve or other physiologically relevant measures. Performing quantitative CMR perfusion after physical exercise was beyond the scope of this study and is an area for future investigation. All evaluations were based on subjective scores by two blinded board-certified cardiologists with >2 y of clinical experience. There were differences between subjective assessments in terms of diagnostic value of images. One of the readers provided more positive assessment of the data. This reader has several years of experience in clinical interpretation of stress perfusion data, while the second reader has only 2 y of experience with limited experience in interpreting stress perfusion. Despite this difference, very similar trends were observed in terms of imaging score between different reconstructions. Although subjective assessment was used in this study for comparison between different reconstructions, further studies are warranted to evaluate quantitative perfusion measures extracted using different reconstruction methods versus microspheres in a control animal model.

Our study has several limitations. No compensation of k-space weighting was used for the reconstruction of radially acquired images (58). Only healthy subjects without any perfusion defects were studied. Therefore, the diagnostic value of each reconstruction method was not evaluated, nor was the diagnostic accuracy of the stress perfusion images. The number of subjects was relatively small. Subjects received multiple contrast injections within each session, which resulted in variations in signal level between different perfusion scans on each day. Although not quantified in this study, regional variations of image quality can be observed for some of our images. Further studies are warranted to characterize the regional quality of these accelerated CMR perfusion protocols. Imaging on two different days results in differences in coil position and slice localization. The order of radial perfusion (day 1) and Cartesian perfusion (day 2) was kept constant for all subjects and could have affected the comparison between the two approaches. However, because the two CMR perfusion protocols within each MR examination were separated by ~30–40 min, the amount of residual contrast in both blood and myocardium before the second CMR perfusion protocol should have been minimized. In the statistical analysis, due to the small sample size, no Bonferroni correction was performed. We note that the limit of $P < 0.05$ for statistical significance might not be strict enough to prevent type 1 errors. Finally, a comparison between pharmacologic and physiologic stress perfusion imaging also warrants further investigation.

CONCLUSION

We have demonstrated the feasibility of accelerated CMR perfusion using radial sampling after physical exercise using a supine ergometer in healthy subjects. For reconstruction of undersampled radial perfusion imaging, NLINV and CG-SENSE resulted in better image quality when compared with conventional gridding or CS-TV regularization. Further technical improvements and clinical assessments are needed before implementing this approach in patients with suspected CAD.

REFERENCES

1. Roger VL, Go AS, Lloyd-Jones DM, et al. Heart disease and stroke statistics—2012 update: a report from the American Heart Association. Circulation 2011;125:e2–e220.
2. Patel MR, Peterson ED, Dai D, Brennan JM, Redberg RF, Anderson HV, Brindis RG, Douglas PS. Low diagnostic yield of elective coronary angiography. N Engl J Med 2010;362:886–895.
3. McNamara MT, Higgins CB, Ehman RL, Revel D, Sievers R, Brasch RC. Acute myocardial ischemia: magnetic resonance contrast enhancement with gadolinium-DTPA. Radiology 1984;153:157–163.
4. Atkinson DJ, Burstein D, Edelman RR. First-pass cardiac perfusion: evaluation with ultrafast MR imaging. Radiology 1990;174:757–762.

5. Jerosch-Herold M, Kwong RY. Optimal imaging strategies to assess coronary blood flow and risk for patients with coronary artery disease. Curr Opin Cardiol 2008;23:599–606.
6. Jerosch-Herold M, Seethamraju RT, Swingen CM, Wilke NM, Stillman AE. Analysis of myocardial perfusion MRI. J Magn Reson Imaging 2004;19:758–770.
7. Wilke N, Jerosch-Herold M, Stillman AE, et al. Concepts of myocardial perfusion imaging in magnetic resonance imaging. Magn Reson Q 1994;10:249–286.
8. Kellman P, Arai AE. Imaging sequences for first pass perfusion—a review. J Cardiovasc Magn Reson 2007;9:525–537.
9. Kim H, Klem I, Kim R. Detection of myocardial ischemia by stress perfusion cardiovascular magnetic resonance. Cardiol Clin 2007;25: 57–70, vi.
10. Pilz G, Jeske A, Klos M, Ali E, Hoefling B, Scheck R, Bernhardt P. Prognostic value of normal adenosine-stress cardiac magnetic resonance imaging. Am J Cardiol 2008;101:1408–1412.
11. Syed M, Paterson D, Ingkanisorn W, Rhoads K, Hill J, Cannon RI, Arai A. Reproducibility and inter-observer variability of dobutamine stress CMR in patients with severe coronary disease: implications for clinical research. J Cardiovasc Magn Reson 2005;7:763–768.
12. Foster EL, Arnold JW, Jekic M, Bender JA, Balasubramanian V, Thavendiranathan P, Dickerson JA, Raman SV, Simonetti OP. MR-compatible treadmill for exercise stress cardiac magnetic resonance imaging. Magn Reson Med 2012;67:880–889.
13. Raman S, Dickerson J, Jekic M, Foster E, Pennell M, McCarthy B, Simonetti O. Real-time cine and myocardial perfusion with treadmill exercise stress cardiovascular magnetic resonance in patients referred for stress SPECT. J Cardiovasc Magn Reson 2010;12:41.
14. Thavendiranathan P, Dickerson J, Scandling D, Balasubramanian V, Hall N, Foster E, Arnold JW, Pennell M, Simonetti OP, Raman SV. Myocardial function and perfusion assessment with exercise stress cardiovascular magnetic resonance using an MRI-compatible treadmill in patients referred for stress SPECT. J Cardiovasc Magn Reson 2012;14(suppl 1):P1.
15. Jekic M, Foster E, Ballinger M, Raman S, Simonetti O. Cardiac function and myocardial perfusion immediately following maximal treadmill exercise inside the MRI room. J Cardiovasc Magn Reson 2008; 10:3.
16. Cheng C, Herfkens R, Taylor C. Inferior vena caval hemodynamics quantified in vivo at rest and during cycling exercise using magnetic resonance imaging. Am J Physiol Heart Circ Physiol 2003;284:H1161–H1167.
17. Cheng C, Herfkens R, Taylor C. Abdominal aortic hemodynamic conditions in healthy subjects aged 50–70 at rest and during lower limb exercise: in vivo quantification using MRI. Atherosclerosis 2003;168: 323–331.
18. Taylor C, Cheng C, Espinosa L, Tang B, Parker D, Herfkens R. In vivo quantification of blood flow and wall shear stress in the human abdominal aorta during lower limb exercise. Ann Biomed Eng 2002; 30:402–408.
19. Niezen R, Doornbos J, van der Wall E, de Roos A. Measurement of aortic and pulmonary flow with MRI at rest and during physical exercise. J Comput Assist Tomogr 1998;22:194–201.
20. Hjortdal V, Emmertsen K, Stenbøg E, Fründ T, Schmidt M, Kromann O, Sørensen K, Pedersen E. Effects of exercise and respiration on blood flow in total cavopulmonary connection: a real-time magnetic resonance flow study. Circulation 2003;108:1227–1231.
21. Cheng ASH, Pegg TJ, Karamitsos TD, Searle N, Jerosch-Herold M, Choudhury RP, Banning AP, Neubauer S, Robson MD, Selvanayagam JB. Cardiovascular magnetic resonance perfusion imaging at 3-Tesla for the detection of coronary artery disease. J Am Coll Cardiol 2007; 49:2440–2449.
22. Kozerke S, Plein S. Accelerated CMR using zonal, parallel and prior knowledge driven imaging methods. J Cardiovasc Magn Reson 2008; 10:29–47.
23. Lyne JC, Gatehouse PD, Assomull RG, Smith GC, Kellman P, Firmin DN, Pennell DJ. Direct comparison of myocardial perfusion cardiovascular magnetic resonance sequences with parallel acquisition. J Magn Reson Imaging 2007;26:1444–1451.
24. Plein S, Radjenovic A, Ridgway J, Barmby D, Greenwood J, Ball S, Sivananthan M. Coronary artery disease: myocardial perfusion MR imaging with sensitivity encoding versus conventional angiography. Radiology 2005;235:423–430.
25. Jung H, Park J, Yoo J, Ye JC. Radial k-t FOCUSS for high-resolution cardiac cine MRI. Magn Reson Med 2010;63:68–78.
26. Jung H, Sung K, Nayak KS, Kim EY, Ye JC. k-t FOCUSS: a general compressed sensing framework for high resolution dynamic MRI. Magn Reson Med 2009;61:103–116.
27. Tsao J, Boesiger P, Pruessmann KP. k-t BLAST and k-t SENSE: dynamic MRI with high frame rate exploiting spatiotemporal correlations. Magn Reson Med 2003;50:1031–1042.
28. Vitanis V, Manka R, Boesiger P, Kozerke S. Accelerated cardiac perfusion imaging using k-t SENSE with SENSE training. Magn Reson Med 2009;62:955–965.
29. Vitanis V, Manka R, Giese D, Pedersen H, Plein S, Boesiger P, Kozerke S. High resolution three-dimensional cardiac perfusion imaging using compartment-based k-t principal component analysis. Magn Reson Med 2011;65:575–587.
30. Otazo R, Kim D, Axel L, Sodickson DK. Combination of compressed sensing and parallel imaging for highly accelerated first-pass cardiac perfusion MRI. Magn Reson Med 2010;64:767–776.
31. Odille F, Cindea N, Mandry D, Pasquier C, Vuissoz PA, Felblinger J. Generalized MRI reconstruction including elastic physiological motion and coil sensitivity encoding. Magn Reson Med 2009;59: 1401–1411.
32. Shin T, Nayak KS, Santos JM, Nishimura DG, Hu BS, McConnell MV. Three-dimensional first-pass myocardial perfusion MRI using a stack-of-spirals acquisition. Magn Reson Med 2013;69:839–844.
33. Adluru G, McGann C, Speier P, Kholmovski EG, Shaaban A, DiBella EVR. Acquisition and reconstruction of undersampled radial data for myocardial perfusion magnetic resonance imaging. J Magn Reson Imaging 2009;29:466–473.
34. Chen L, Adluru G, Schabel MC, McGann C, DiBella E. Myocardial perfusion MRI with an undersampled 3D stack-of-stars sequence. Med Phys 2012;39:5204–5211.
35. Ge L, Kino A, Griswold M, Carr JC, Li D. Free-breathing myocardial perfusion MRI using SW-CG-HYPR and motion correction. Magn Reson Med 2010;64:1148–1154.
36. Ge L, Kino A, Griswold M, Mistretta C, Carr JC, Li D. Myocardial perfusion MRI with sliding-window conjugate-gradient HYPR. Magn Reson Med 2009;62:835–839.
37. Cooper MA, Nguyen TD, Spincemaille P, Prince MR, Weinsaft JW, Wang Y. Flip angle profile correction for T(1) and T(2) quantification with look-locker inversion recovery 2D steady-state free precession imaging. Magn Reson Med 2012;68:1579–1585.
38. Kholmovski EG, DiBella EVR. Perfusion MRI with radial acquisition for arterial input function assessment. Magn Reson Med 2007;57:821–827.
39. Salerno M, Sica C, Kramer CM, Meyer CH. Improved first-pass spiral myocardial perfusion imaging with variable density trajectories. Magn Reson Med 2013;70:1369–1379.
40. Salerno M, Sica CT, Kramer CM, Meyer CH. Optimization of spiral-based pulse sequences for first-pass myocardial perfusion imaging. Magn Reson Med 2011;65:1602–1610.
41. Adluru G, Chen L, DiBella EV. Undersampled Free Breathing Cardiac Perfusion MRI Reconstruction Without Motion Estimation. In Proceedings of the 8th IEEE International Symposium on Biomedical Imaging: From Nano to Macro, Chicago, Illinois, USA, 2011. p. 97–100.
42. Sharif B, Dharmakumar R, LaBounty T, Arsanjani R, Shufelt C, Thomson L, Bairey Merz CN, Berman DS, Li D. Towards elimination of the dark-rim artifact in first-pass myocardial perfusion MRI: removing gibbs ringing effects using optimized radial imaging. Magn Reson Med 2014;72:124–136.
43. Schuelke C, Roujol S, Foppa M, Gervino EV, Kissinger KV, Goddu B, Berg S, Kozerke S, Manning WJ, Nezafat R. Comparison of reconstruction methods for accelerated cardiac MR stress perfusion after physical stress with supine ergometer. Proceedings of the 21st Annual Meeting if ISMRM, Salt Lake City, Utah, USA, 2013. p. 1318.
44. Basha TA, Roujol S, Kissinger KV, Goddu B, Berg S, Manning WJ, Nezafat R. Free-breathing cardiac MR stress perfusion with real-time slice tracking. Magn Reson Med 2014;72:689–698.
45. Fessler JA, Sutton BP. Nonuniform fast Fourier transfoms using min-max interpolation. IEEE Trans Signal Process 2003;51:560–574.
46. Pruessmann KP, Weiger M, Boernert P, Boesiger P. Advances in SENSE with arbitrary k-space trajectories. Magn Reson Med 2001;46: 638–651.

47. Block KT, Uecker M, Frahm J. Undersampled radial MRI with multiple coils. Iterative image reconstruction using a total variation constraint. Magn Reson Med 2007;57:1086–1098.
48. Kaasschieter E. Preconditioned conjugate gradients for solving singular systems. J Comput Appl Math 1988;24:265–275.
49. Qu P, Zhong K, Zhang B, Wang J, Shen GX. Convergence behavior of iterative SENSE reconstruction with non-Cartesian trajectories. Magn Reson Med 2005;54:1040–1045.
50. Lustig M, Donoho D, Pauly JM. Sparse MRI: the application of compressed sensing for rapid MR imaging. Magn Reson Med 2007;58: 1182–1195.
51. Uecker M, Hohage T, Block KT, Frahm J. Image reconstruction by regularized nonlinear inversion—joint estimation of coil sensitivities and image content. Magn Reson Med 2008;60:674–682.
52. Pedersen H, Kelle S, Ringgaard S, Schnackenburg B, Nagel E, Nehrke K, Kim WY. Quantification of myocardial perfusion using free-breathing MRI and prospective slice tracking. Magn Reson Med 2009; 61:734–738.
53. Moghari MH, Hu P, Kissinger KV, Goddu B, Goepfert L, Ngo L, Manning WJ, Nezafat R. Subject-specific estimation of respiratory navigator tracking factor for free-breathing cardiovascular MR. Magn Reson Med 2012;67:1665–1672.
54. Sharma S, Fong C, Tzung B, Law M, Nayak K. Clinical image quality assessment of accelerated magnetic resonance neuroimaging using compressed sensing. Invest Radiol 2013;48:638–645.
55. Pruessmann KP. Encoding and reconstruction in parallel MRI. NMR Biomed 2006;19:288–299.
56. Usman M, Atkinson D, Odille F, Kolbitsch C, Vaillant G, Schaeffter T, Batchelor PG, Prieto C. Motion corrected compressed sensing for free-breathing dynamic cardiac MRI. Magn Reson Med 2013;70:504–516.
57. Pipe J. Motion correction with PROPELLER MRI: application to head motion and free-breathing cardiac imaging. Magn Reson Med 1999; 42:963–969.
58. Song HK, Dougherty L. k-space weighted image contrast (KWIC) for contrast manipulation in projection reconstruction MRI. Magn Reson Med 2000;44:825–832.